# Supporting Information: *In-situ* Simultaneous Photovoltaic and Structural Evolution of Perovskite Solar Cells During Film Formation

Mejd Alsari[1], Oier Bikondoa[2], James Bishop[3], Mojtaba Abdi-Jalebi[1], Lütfiye Y. Ozer[4], Mark Hampton[5], Paul Thompson[6], Maximilian Hoerantner[7], Suhas Mahesh[7], Claire Greenland[3], J. Emyr Macdonald[5], Giovanni Palmisano[4], Henry J. Snaith[7], David G. Lidzey[3], Samuel D. Stranks[1], Richard H. Friend[1], Samuele Lilliu[3,8*]

[1] Cavendish Laboratory, University of Cambridge, CB30HE Cambridge, UK

[2] Department of Physics, University of Warwick, CV4 7AL Coventry, UK

[3] Department of Physics and Astronomy, University of Sheffield, Sheffield, S3 7RH, UK

[4] Department of Chemical Engineering, Khalifa University of Science and Technology, Masdar Institute, PO BOX 54224, Abu Dhabi, UAE

[5] School of Physics and Astronomy, Cardiff University, CF24 3AA Cardiff, UK

[6] University of Liverpool, Oliver Lodge, Oxford Street, Liverpool, L69 7ZE

[7] Clarendon Laboratory, Department of Physics, University of Oxford, OX1 3PU Oxford, UK

[8] The UAE Centre for Crystallography, UAE

[*] Correspondence to: s.lilliu@sheffield.ac.uk (or samuele_lilliu@hotmail.it)

## Table of contents

## Setup Illustration

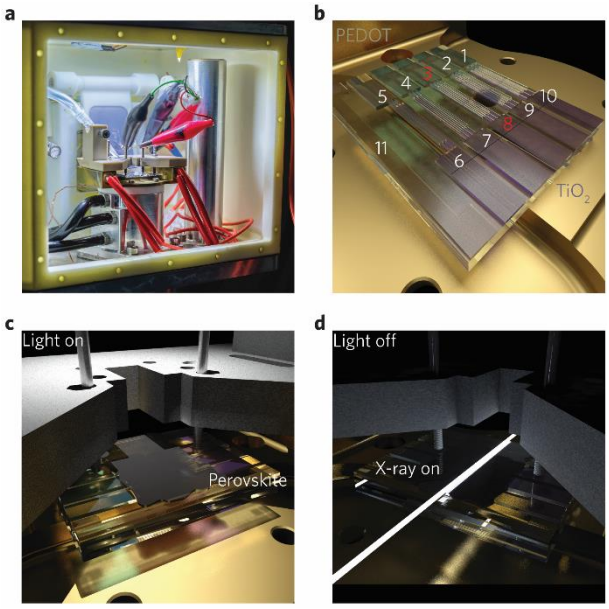


Figure S1| | Illustration of the measurements setup. a, Annealing chamber. b, Illustration of ITO interdigitated substrate electrodeposited with PEDOT (electrodes 1-5) and $TiO_2$ (electrodes 6-10). Electrode 11 is bare ITO. c, Illustration of the experimental setup for current-voltage sweeps performed *in-situ* without X-rays. d, Illustration of the setup for diffraction pattern measurement (light off) with a 10 keV X-ray at grazing incidence.

## Summary of measured IBC solar cells

Table S1 | Summary of IBC measurements details. $T_a$ is the annealing temperature, $t_{max}$ is the total measurement period for the data shown in the graphs, $D_L$ is the light dose in seconds per minute, $D_{XRD}$ is the X-ray dose in seconds/minutes, $\Delta T$ is the duration of a measurement loop step in seconds, $\Delta T_L$ is the time the sample is exposed to light during a loop step, $\Delta T_{XRD}$ is the time the sample is exposed to X-rays during a loop step, MS is the measurement step. FD: forward *JV* under dark, RL: reverse *JV* under light.

| Sample name | Additive | $T_a$ [°C] | $t_{max}$ [min] | $D_L$ [s/min] | $D_{XRD}$ [s/min] | $\Delta T$ [s] | $\Delta T_L$ [s] | $\Delta T_{XRD}$ [s] | MS | Notes |
|---|---|---|---|---|---|---|---|---|---|---|
| S130 | HI | 88.2 | 189 | 19.9 | 1.1 | 54.4 | 18.0 | 1 | XRD, FD, RL | |
| S28 | HI | 88.2 | 186 | 19.9 | 11 | 54.4 | 18.0 | 10 | XRD, FD, RL | |
| S29 | HI | 88.2 | 184 | 19.9 | 11 | 54.4 | 18.0 | 10 | XRD, FD, RL | No selective electrodes |
| S142 | HI | 83.8 | 123 | 19.9 | 1.1 | 54.4 | 18.0 | 1 | XRD, FD, RL | |
| S129 | HI | 92.5 | 190 | 19.9 | 1.1 | 54.4 | 18.0 | 1 | XRD, FD, RL | |
| S128 | HI | 96.8 | 190 | 19.9 | 1.1 | 54.4 | 18.0 | 1 | XRD, FD, RL | |
| S132 | HI | 88.2 | 193 | 2.0 | 0.1 | 600 | 18.0 | 1 | XRD, FD, RL | |
| S116 | HI | 88.2 | 213 | 0.6 | 1.1 | 600 | 6 | 10 | XRD, $J_{sc}$, $V_{oc}$ | |
| S117 | HI | 88.2 | 217 | 6.6 | 11 | 54.4 | 6 | 10 | XRD, $J_{sc}$, $V_{oc}$ | |
| S115 | HI | 88.2 | 190 | 19.9 | 11 | 54.4 | 18 | 10 | XRD, FD, RL | |
| S113 | HI | 88.2 | 190 | 39.8 | 11 | 54.4 | 36 | 10 | XRD, FL, RL | |
| S131 | HI | 88.2 | 92 | 0 | 5.5 | 11 | 0 | 1 | XRD | No light |
| S105 | HI | 96.8 | 196 | 6.6 | 0 | 54.4 | 6 | 0 | $J_{sc}$, $V_{oc}$ | Offline |
| S139 | $PbI_2$ | 83.8 | 123 | 19.9 | 1.1 | 54.4 | 18.0 | 1 | XRD, FD, RL | |
| S137 | $PbI_2$ | 92.5 | 95 | 19.9 | 1.1 | 54.4 | 18.0 | 1 | XRD, FD, RL | |
| S158 | $PbI_2$ | 114.7 | 83 | 19.9 | 1.1 | 54.4 | 18.0 | 1 | XRD, FD, RL | |
| S135 | $PbI_2$ | 101.6 | 92 | 0 | 5.5 | 11 | 0 | 1 | XRD | No light |

## IBC solar cells with and without selective electrodes

In Figure S2 we show a comparison between the current-voltage sweeps under light (Figure S2a) and dark (Figure S2b) conditions of a device coated with PEDOT and $TiO_2$ (S28) and an uncoated device (S29). Sweeps are shown at three different instants of the *in-situ* anneal at 88.2°C. The uncoated devices do not show any photovoltaic behaviour (Figure S2a). The coated device shows a typical photovoltaic diode-like behaviour. Dark currents are three orders of magnitude smaller than light currents. The dynamics of the perovskite peak integral evolution is identical between the coated and the uncoated IBC solar cells. A comparison point by point of the diffraction patterns, the peak integrals, and the JV sweeps is available in Movie S1, S28 and S29.

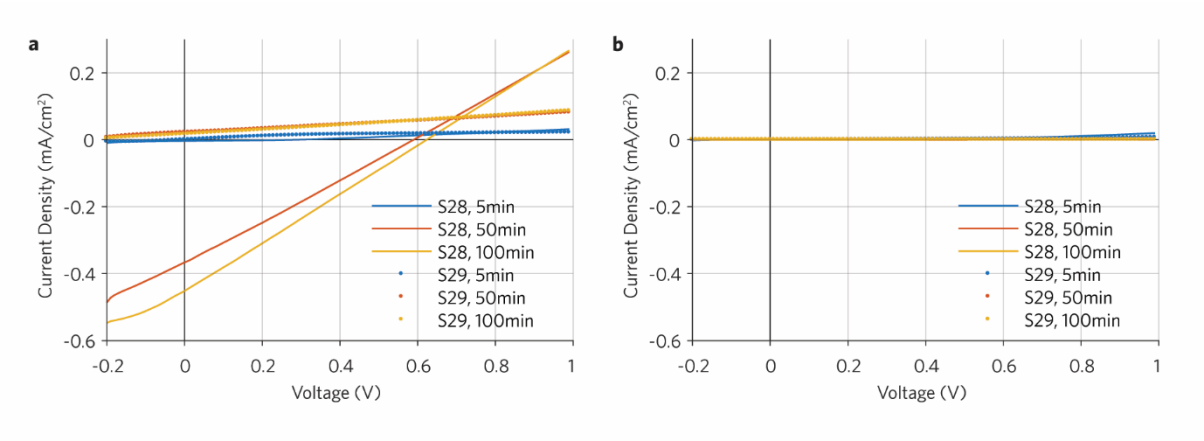


Figure S2 | Comparison of current-voltage sweeps between IBC solar cells with (S28) and without selective electrodes (S29) during the *in-situ* anneal at 88.2°C (MAI:$PbCl_2$ + HI). a, Forward JV sweeps under light conditions. b, Forward JV sweeps under dark conditions. The measurement procedure for the two IBC solar cells was: measure one GI-WAXS pattern (10s integration time), Forward JV sweep (18s, light off), Reverse JV sweep (18s, light off), repeat every 54.4s.

## Comparison with Pazos *et al.*

Dark and light currents of the coated device IBC S28 show a trend similar to the one reported by Pazos *et al.* (*cf.* Fig. S14 and S15).[1] Pazos et al. reported on the same perovskite employed in our work, but spin-coated from a different precursor solution (MAI: $PbAc_2$) and annealed at 100°C.[1] Their interdigitated IBC solar cells had a channel gap of 4 μm, while here were report on IBC solar cells having a gap of 100μm. The active area employed by Pazos *et al.* (0.096 $cm^2$) was calculated as in our work, without employing a shadow mask (Figure S32). In the *JV* measurements reported in Fig. S14[1], Pazos *et al.* show a comparison between *JV* sweeps with and without a 2V pre-biasing lasting 30s. In our work, we did not apply any pre-biasing before the *JV* sweeps. The figures-of-merit extracted from Fig. S14 (no pre-bias) are: $V_{oc} \approx 0.5$ V, $J_{sc} \approx 0.03$ mA/$cm^2$, $PCE \approx 0.004\%$, $FF \approx 0.2$. The figures-of-merit for S28, for example, after 100min are: $V_{oc} \approx 0.62$ V, $J_{sc} \approx 0.45$ mA/$cm^2$, $PCE \approx 0.07\%$, $FF \approx 0.25$. The counterintuitively superior performance of the 100 μm gap devices shown here compared to the 4 μm gap devices could be attributed to the employment of $PbCl_2$ in the precursor solution, which results in a favourable morphology of the final $CH_3NH_3PbI_3$ perovskite film and longer electron diffusion lengths.[2]

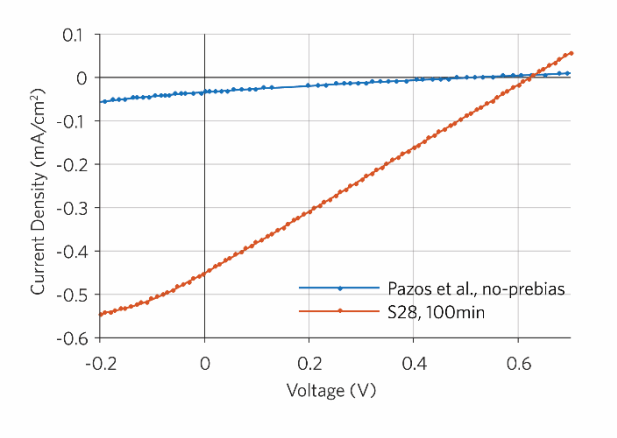


Figure S3 | Comparison between IBC reported by Pazos *et al.* and IBC reported in this work (MAI:$PbCl_2$ + HI). *JV* data from Pazos *et al.* was extracted from Fig. S14 in ref. [1]. Pazos *et al.* report on perovskite IBC solar cells spin-coated from MAI: $PbAc_2$ and measured at room temperature. The *JV* data from S28 corresponds to the measurement performed at 88.2°C, 100min after the beginning of the anneal.

## Different channel lengths and electrode combinations

Measurements performed on couples of electrodes having different channel lengths (Figure S4) did not show any statistically relevant trend in the figures-of-merit vs channel length (Figure S5).

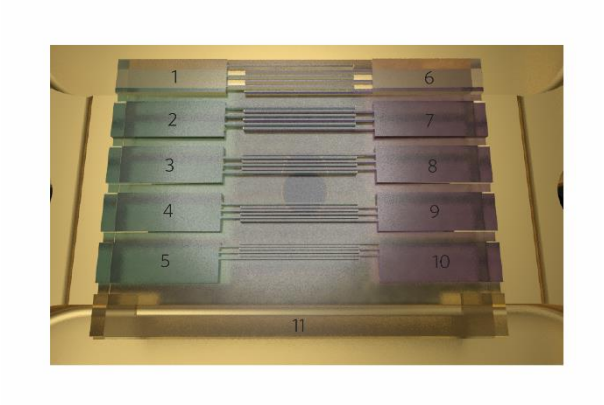


Figure S4 | Schematics of the electrodes numbering and gap between digits in IBC solar cells. Electrodes 1 and 6: 200 µm; electrodes 2 and 7: 150 µm; electrodes 3 and 8: 100 µm; electrodes 4 and 9: 75 µm; electrodes 5 and 10: 50 µm.

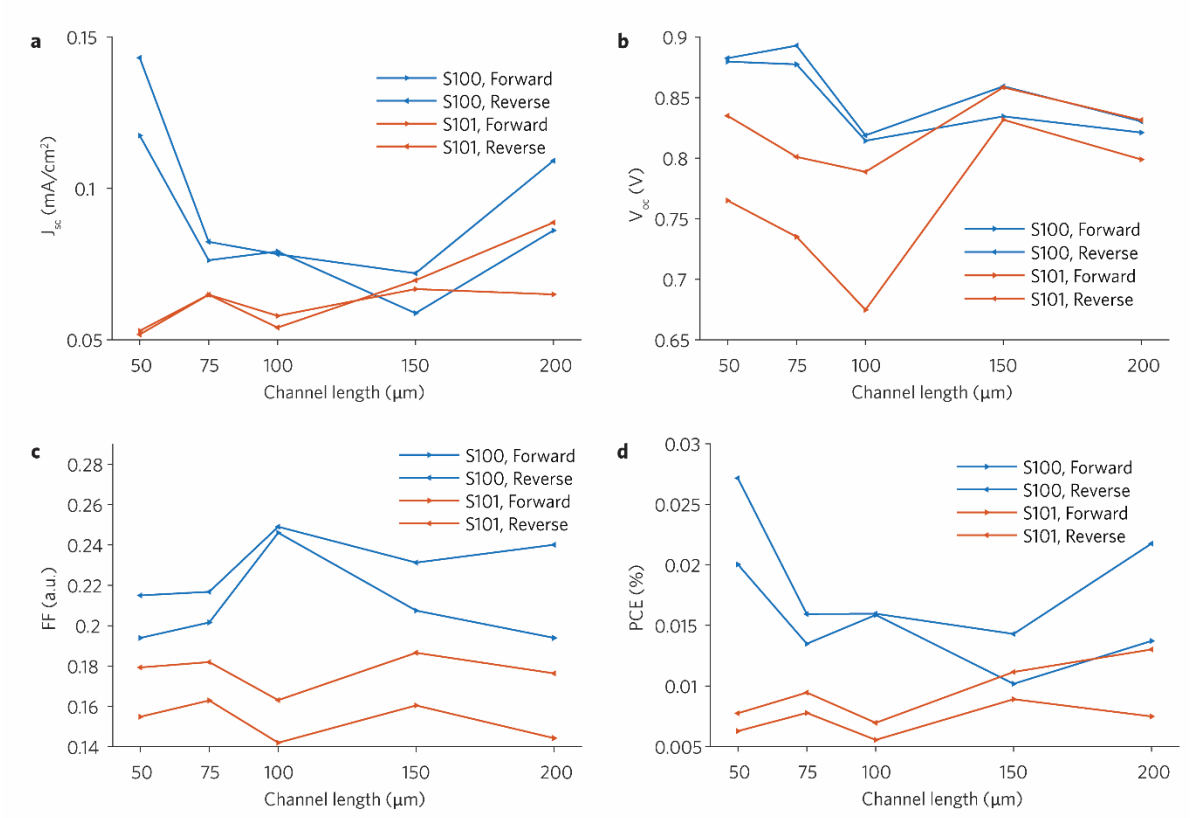


Figure S5 | Figures-of-merit of two IBC solar cells vs channel length (MAI:$PbCl_2$ + HI). Both solar cells were measured offline without X-rays. The FOM shown for each channel length of S100 and S101 were acquired at room temperature with a forward scan followed by a reverse scan (waiting time 5min between measurements).

Figure S6 shows a series of measurements performed by connecting electrodes belonging to different couples of interdigitated electrodes. IBC S103 was annealed at 88.2°C while performing only static $V_{oc}$ and $J_{sc}$ measurements. The latest probed $V_{oc}$ and $J_{sc}$ between electrodes 3 and 8 (100 µm) were 0.28 V and 0.039 mA/cm$^2$. The *JV* sweeps measured across electrodes 3 and 7 (S103c) show a measurable photocurrent two orders of magnitude smaller than the one measured across the 100 µm gap. We were not able to measure any photocurrent between electrode 2 and electrode 11 (bare ITO).

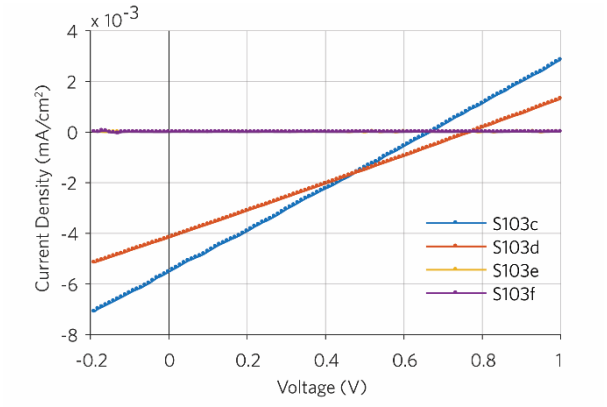


Figure S6 | Reverse JV sweeps under light measured across electrodes not facing each other (MAI:$PbCl_2$ + HI). The reverse *JV* sweeps shown were performed at 88.2°C. S103c, S103d, S104e, and S103f were measured across electrodes 3 and 7, 2 and 7, 2 and floating, 2 and 11.

## Non-Zero $V_{oc}$ in the Precursor Phase

Table S2 | Open circuit voltage measurements on IBC solar cells before perovskite full conversion. $T_a$ is the annealing temperature, $t_1$ is the instant at which the measurement ( $V_{oc}$ at $t_1$) was performed since the IBC solar cell was placed on the hotplate (with the exception of S102, which is not annealed).

| Sample name | Perovskite System | $T_a$ [°C] | $t_1$ [min] | $V_{oc}$ at $t_1$ [V] |
|---|---|---|---|---|
| S102 | MAI:$PbCl_2$ + HI | Room temperature | 3 | 0.52 |
| S9 | MAI: $PbAc_2$ | 96.8 | 3.8 | 0.65 |
| S27 | MAI: $PbAc_2$ | 88.2 | 2.7 | 0.28 |
| S155 | $Cs_{0.5}(MA_{0.17}FA_{0.83})_{0.95}Pb(I_{0.83}Br_{0.17})_3$ | 83.8 | 2.2 | 0.68 |
| S156 | $Cs_{0.5}(MA_{0.17}FA_{0.83})_{0.95}Pb(I_{0.83}Br_{0.17})_3$ | 92.5 | 5.0 | 0.28 |
| S157 | $Cs_{0.5}(MA_{0.17}FA_{0.83})_{0.95}Pb(I_{0.83}Br_{0.17})_3$ | 101.6 | 3.3 | 0.39 |
| S119 | $(FAI)_{1.0}(MABr)_{0.2}(PbI_2)_{1.1}(PbBr_2)_{0.20}$ | 88.2 | 2.8 | 0.81 |
| S120 | $(FAI)_{1.0}(MABr)_{0.2}(PbI_2)_{1.1}(PbBr_2)_{0.20}$ | 96.8 | 2.8 | 0.54 |
| S121 | $(FAI)_{1.0}(MABr)_{0.2}(PbI_2)_{1.1}(PbBr_2)_{0.20}$ | 101.6 | 3.1 | 0.42 |
| S122 | $(FAI)_{1.0}(MABr)_{0.2}(PbI_2)_{1.1}(PbBr_2)_{0.20}$ | 101.6 | 2.9 | 0.38 |
| S123 | $(FAI)_{1.0}(MABr)_{0.2}(PbI_2)_{1.1}(PbBr_2)_{0.20}$ | 101.6 | 3.1 | 0.34 |
| S125 | $(FAI)_{1.0}(MABr)_{0.2}(PbI_2)_{1.1}(PbBr_2)_{0.20}$ | 101.6 | 2.9 | 0.48 |

## IBC S142 annealed at 83.8°C

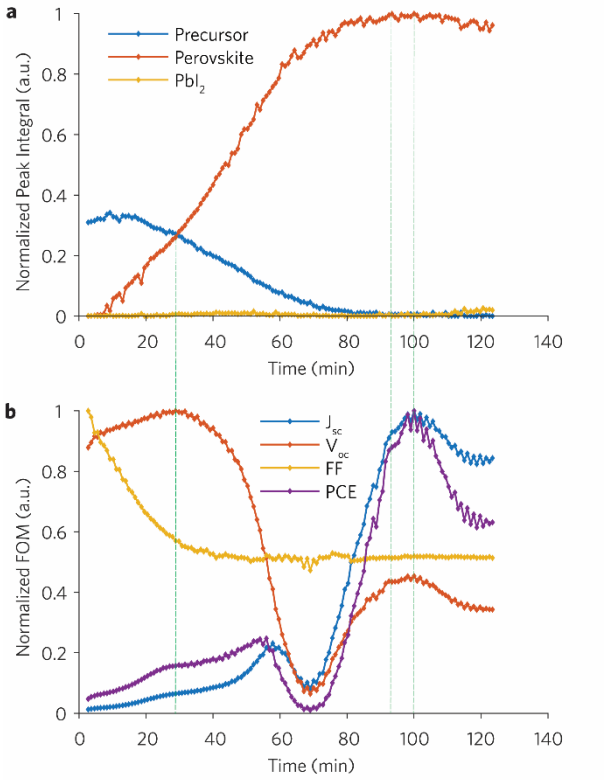


Figure S7 | Structural and opto-electrical parameters extracted from simultaneous GI-WAXS diffraction patterns (dark) and current-voltage (light) measurement of a ($MAI:PbCl_2 + HI$) IBC solar cell (S142) during *in-situ* anneal at 83.8°C. a, Integrated precursor, perovskite and $PbI_2$ peak intensities vs annealing time b, Normalized figures-of-merit (FOM) vs annealing time. The following measurement loop step was repeated every 54.4s: measure one GI-WAXS pattern (1s integration time), forward JV sweep (18s, light off), reverse JV sweep (18s, light on).

## IBC S129 annealed at 92.5°C

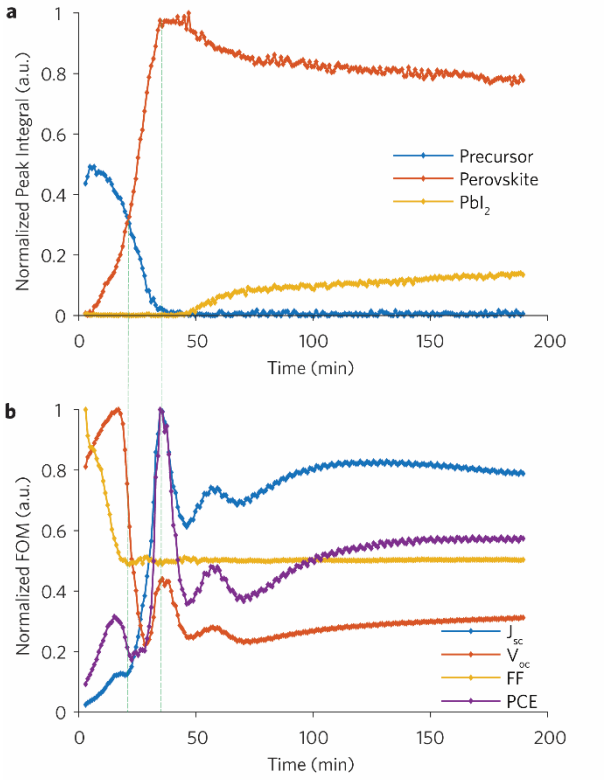


Figure S8 | Structural and opto-electrical parameters extracted from simultaneous GI-WAXS diffraction patterns (dark) and current-voltage (light) measurement of a ($MAI:PbCl_2 + HI$) IBC solar cell (S129) during *in-situ* anneal at 92.5°C. a, Integrated precursor, perovskite and $PbI_2$ peak intensities vs annealing time b, Normalized figures-of-merit (FOM) vs annealing time. The following measurement loop step was repeated every 54.4s: measure one GI-WAXS pattern (1s integration time), forward JV sweep (18s, light off), reverse JV sweep (18s, light on).

## IBC S128 annealed at 96.8°C

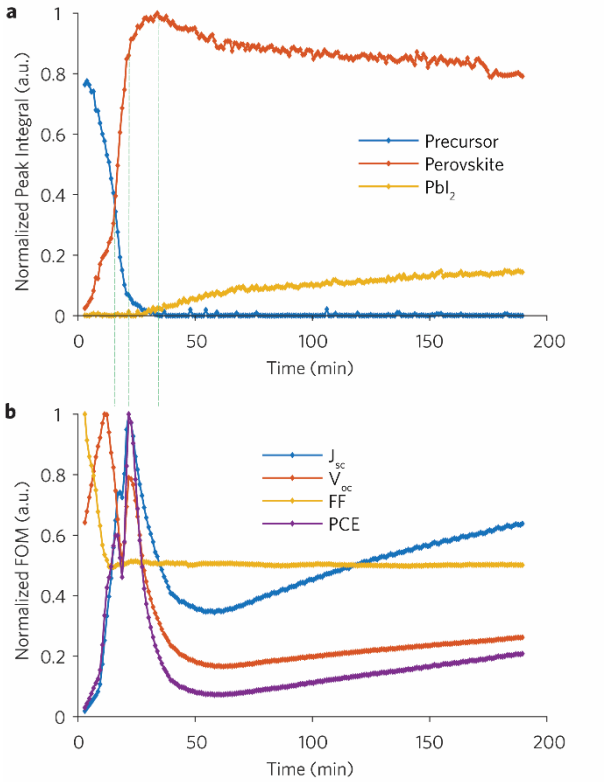


Figure S9 | Structural and opto-electrical parameters extracted from simultaneous GI-WAXS diffraction patterns (dark) and current-voltage (light) measurement of a ($MAI:PbCl_2 + HI$) IBC solar cell (S128) during *in-situ* anneal at 96.8°C. a, Integrated precursor, perovskite and $PbI_2$ peak intensities vs annealing time b, Normalized figures-of-merit (FOM) vs annealing time. The following measurement loop step was repeated every 54.4s: measure one GI-WAXS pattern (1s integration time), forward JV sweep (18s, light off), reverse JV sweep (18s, light on).

## Comparison between IBC S142 (83.8°C), S130 (88.2°C), S129 (92.5°C) and S128 (96.8°C)

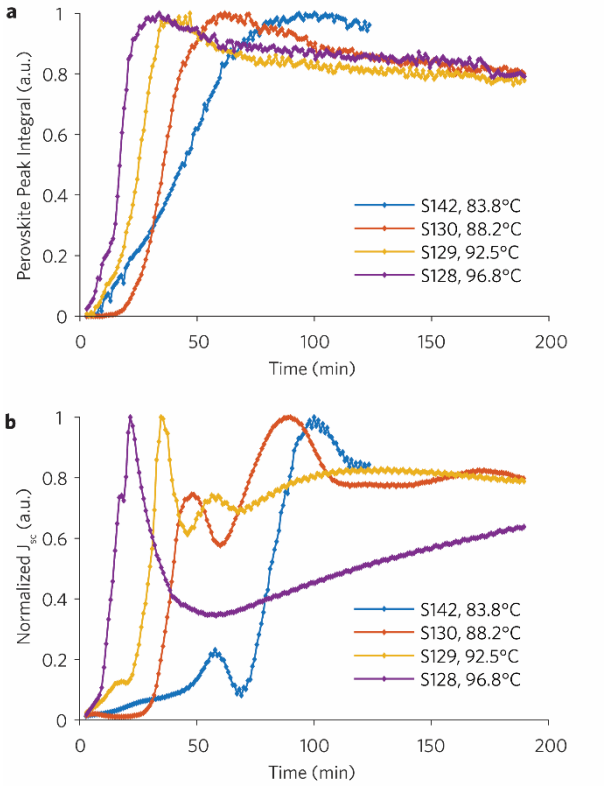


Figure S10 | Comparison between perovskite peak integral and normalized $J_{sc}$ for (MAI:$PbCl_2$ + HI) IBC solar cells annealed *in-situ* at different temperatures.

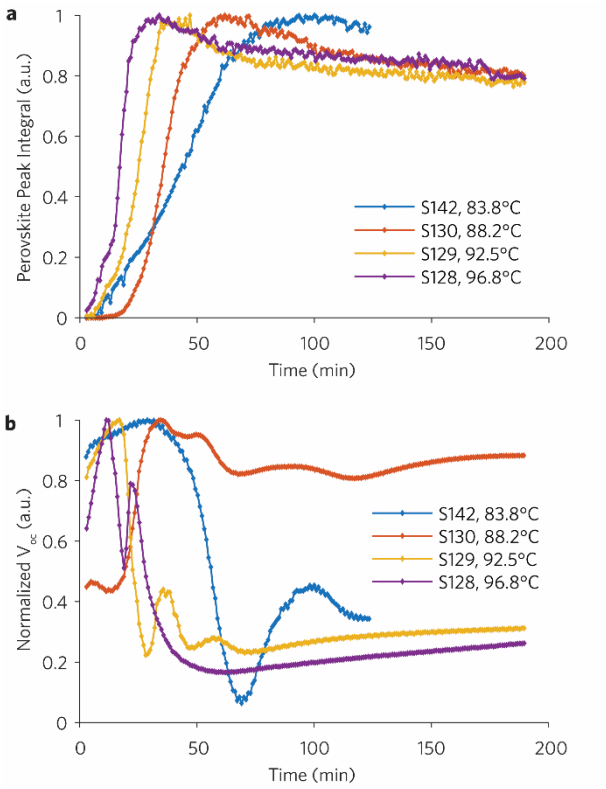


Figure S11 | Comparison between perovskite peak integral and normalized $V_{oc}$ for (MAI:$PbCl_2$ + HI) IBC solar cells annealed *in-situ* at different temperatures .

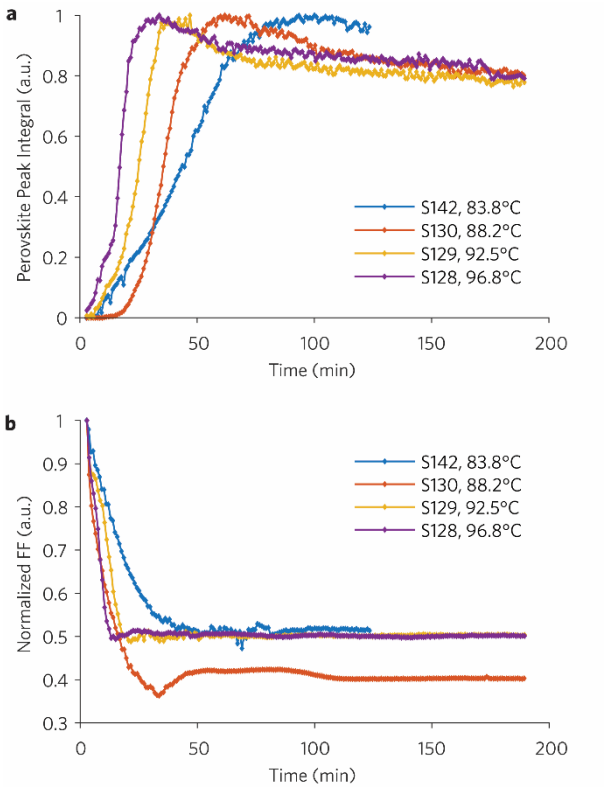


Figure S12 | Comparison between perovskite peak integral and normalized FF for (MAI:$PbCl_2$ + HI) IBC solar cells annealed *in-situ* at different temperatures .

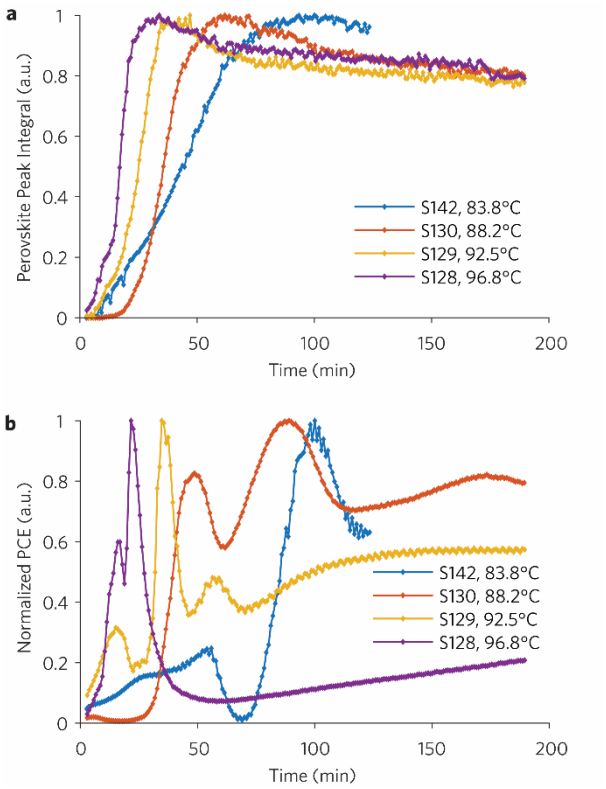


Figure S13 | Comparison between perovskite peak integral and normalized PCE for (MAI:$PbCl_2$ + HI) IBC solar cells annealed *in-situ* at different temperatures .

## JMA analysis (HI additive)

The kinetics of the precursor to perovskite transformation and peroskite to $PbI_2$ degradation processes can be estimated with the Johnson-Mehl-Avrami (JMA) model.[3-5] If normalized perovskite integrals are indicated as $x(t)$:

$$\ln(t_{x2} - t_{x1}) = \frac{E_a}{RT} - \ln k_0 + \ln(\beta_{x2} - \beta_{x1})$$
$$x(t) = 1 - \exp\left[-\left(k_0 t \exp\left(-\frac{E_a}{RT}\right)\right)^n\right] \quad (1)$$

where $t_{x1}$ and $t_{x2}$ are the time at which the transformed fraction is $x_1$ and $x_2$, $E_a$ is the effective activation energy, $R$ is the gas constant, $T$ is the temperature, $k_0$ is the rate constant prefactor, $n$ is the growth constant, and $\beta_{xn}$ is a state property.[6] Figure S14a shows data-points from the normalized perovskite peak integrals extracted from IBC solar cells annealed at different temperatures. Figure S14b shows plots of $\ln(t_{x2}- t_{x1})$, where $t_{x2}$ corresponds to the instants when $x(t)$ is 0.8 and $t_{x1}$ corresponds to the instants when $x(t)$ is 0. From the slope of the line in eq. (1) we obtain an activation energy of 89±12 kJ/mol. The concept of activation energy used by Moore *et al.* and here should not be taken in absolute terms, i.e. it provides a means of comparing the speed of crystallization between different materials. The activation energy extracted in Figure S14b is then used to fit the data-points in Figure S14a with the sigmoidal curve represented by eq. (1). The extracted $k_0$ and $n$ parameters are reported in Table S3. As highlighted by Moore *et al.* the JMA model only offers a good mathematical description of the system and $k_0$ and $n$ should be treated as empirical fit parameters.

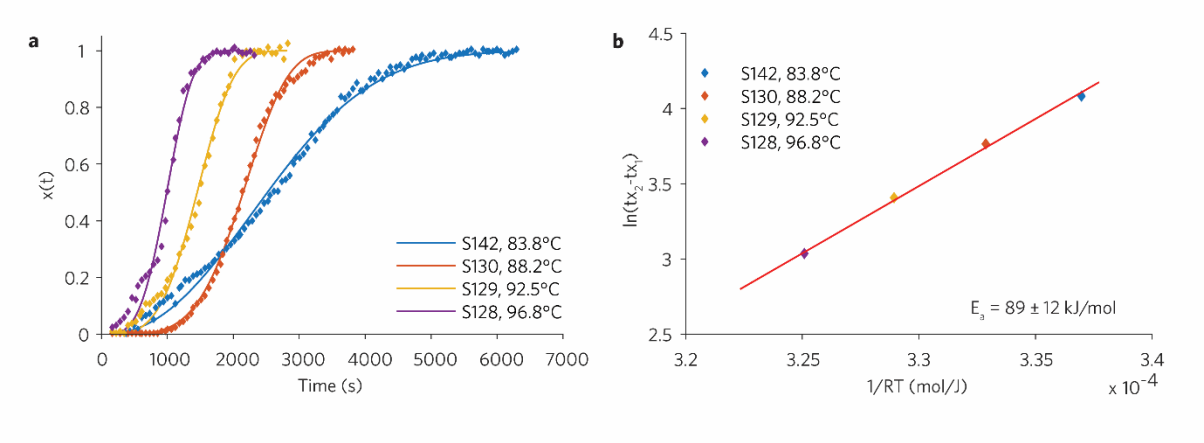


Figure S14 | Kinetic data for isothermally annealed (MAI:$PbCl_2$ + HI) IBC perovskite solar cells. a, plots of the perovskite peak integral extracted from azimuthally integrated line profiles for isothermally annealed perovskite solar cells at 83.8°C (blue diamonds), 88.2°C (red diamonds), 92.5°C (yellow diamonds), 96.8°C (violet diamonds), with the JMA model fits (sigmoid in eq. 1, solid lines). b, plots constructed as described in the text and fitted with the line in eq. 1, to extract the slope corresponding to the activation energy $E_a$.

Table S3 | Parameters extracted from the sigmoidal fit of x(*t*) datapoints in Figure S14a using an activation energy of 89 kJ/mol. $R^2$ is the goodness of the fit.

| **Anneal Temperature (°C)** | ***n*** **(a.u.)** | $k_0$ **(a.u.)** | $R^2$ **(a.u.)** |
|---|---|---|---|
| **83.8** | 2.28±0.06 | $(4.07\pm0.03) \times 10^9$ | 0.996 |
| **88.2** | 4.53±0.15 | $(3.58\pm0.02) \times 10^9$ | 0.998 |
| **92.5** | 3.79±0.24 | $(3.68\pm0.05) \times 10^9$ | 0.994 |
| **96.8** | 3.64±0.35 | $(3.81\pm0.08) \times 10^9$ | 0.989 |

## IBC S132 annealed at 88.2°C

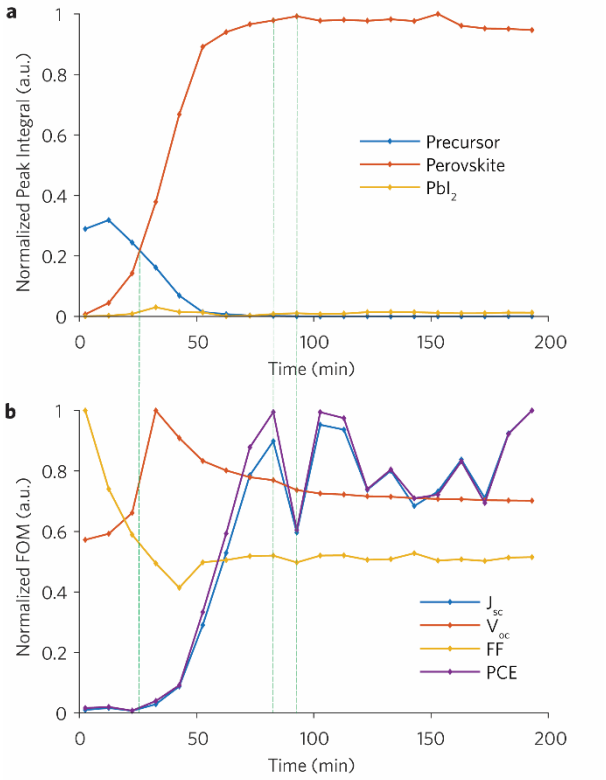


Figure S15 | Structural and opto-electrical parameters extracted from simultaneous GI-WAXS diffraction patterns (dark) and current-voltage (light) measurement of (MAI:PbCl2 + HI) IBC solar cell (S132) during *in-situ* anneal at 88.2°C. a, Integrated precursor, perovskite and $PbI_2$ peak intensities vs annealing time b, Normalized figures-of-merit (FOM) vs annealing time. The following measurement loop step was repeated every 10min: measure one GI-WAXS pattern (1s integration time), forward JV sweep (18s, light off), reverse JV sweep (18s, light on).

## IBC S116 annealed at 88.2°C

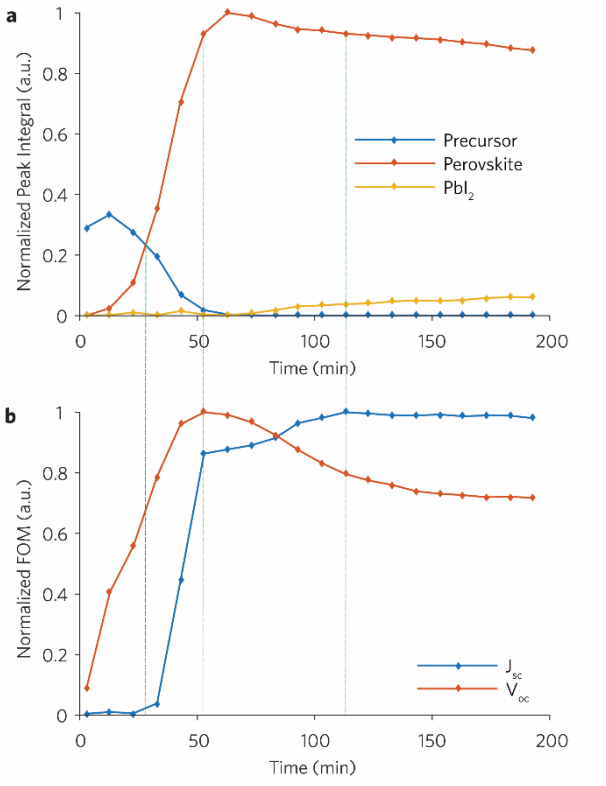


Figure S16 | Structural and opto-electrical parameters extracted from simultaneous GI-WAXS diffraction patterns (dark) and current-voltage (light) measurement of (MAI:PbCl2 + HI) IBC solar cell (S116) during *in-situ* anneal at 88.2°C. a, Integrated precursor, perovskite and $PbI_2$ peak intensities vs annealing time b, Normalized figures-of-merit (FOM) vs annealing time. The following measurement loop step was repeated every 10min: measure one GI-WAXS pattern (10s integration time), static $J_{sc}$ (3s, light off), static $V_{oc}$ (3s, light on).

## IBC S117 annealed at 88.2°C

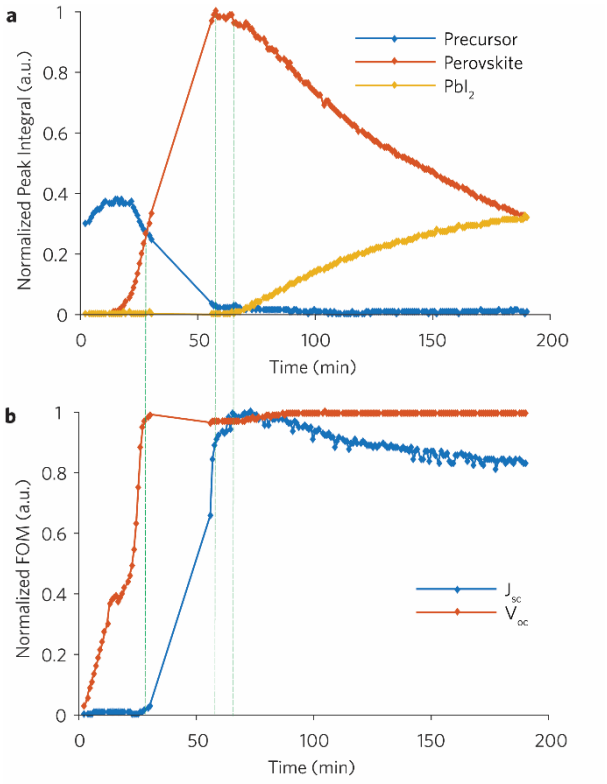


Figure S17 | Structural and opto-electrical parameters extracted from simultaneous GI-WAXS diffraction patterns (dark) and current-voltage (light) measurement of (MAI:PbCl2 + HI) IBC solar cell (S117) during *in-situ* anneal at 88.2°C. a, Integrated precursor, perovskite and $PbI_2$ peak intensities vs annealing time b, Normalized figures-of-merit (FOM) vs annealing time. The following measurement loop step was repeated every 54.4s: measure one GI-WAXS pattern (10s integration time), static $J_{sc}$ (3s, light off), static $V_{oc}$ (3s, light on).

## Beam damage

Perovskite films suffer from both X-ray and light damage. Beam damage is directly proportional to the X-ray dose. The dose depends on how long is the sample exposed to the X-ray beam and on the X-ray flux. Beam damage is also stronger in the presence of both oxygen and moisture.[4,7]

In Figure S18, we show pictures of six IBC solar cells measured *in-situ* under different conditions illustrated in Table S1. Beam damage is clearly visible as a yellow footprint in the IBC solar cells exposed to an overall beam exposure exceeding 4min (Figure S18d-f).

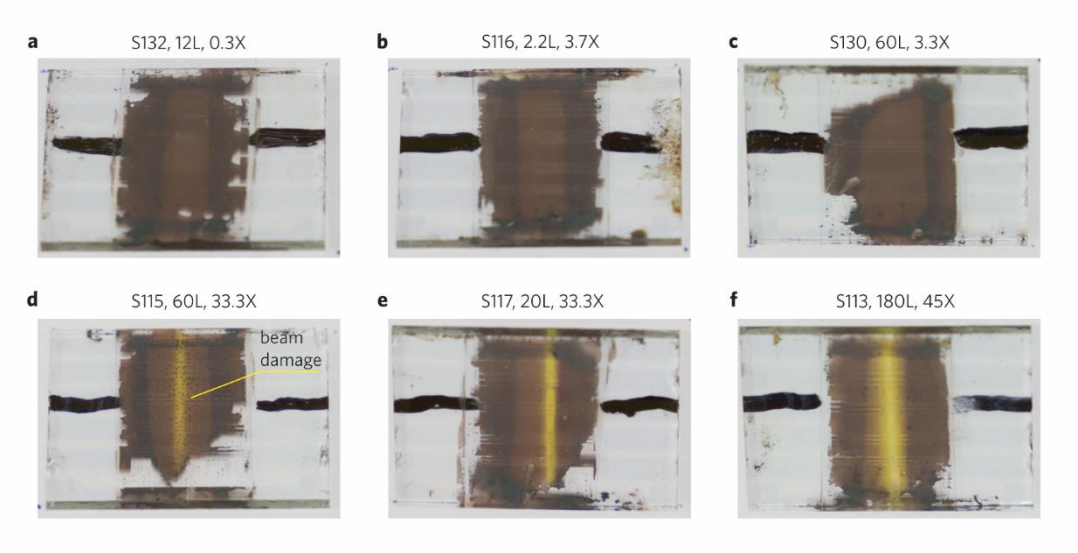


Figure S18 | Pictures of the (MAI:PbCl2 + HI) IBC solar cells after the GI-WAXS and JV measurements *in-situ* during the anneal at 90°C. The figures title indicate the IBC sample name, the overall light exposure in minutes followed by 'L', and the overall X-ray exposure in minutes followed by 'X'. The black marks indicate the position of the cathode and anode where the electrical probes were connected for the *JV* sweeps. The yellow portions of the film are made of perovskite degraded into $PbI_2$, as the effect of beam damage.

The impact of X-ray beam damage can be quantified by looking at how the intensity of the perovskite or $PbI_2$ diffraction rings decrease and increase, respectively, over time during the GI-WAXS and the *JV* measurements *in-situ* during the anneal at 88.2°C. Figure S19**a** shows plots of the perovskite peak integral vs annealing time for 7 IBC solar cells measured under different conditions**.** The trend up to ~50min is similar for all samples, suggesting that the perovskite film is unaffected by beam damage until a complete precursor to perovskite conversion has taken place. However, after ~50min there is a clear difference between the IBC solar cells exposed to a high X-ray dose (>1.1 s/min) and the ones exposed to a lower X-ray dose ( ≤1.1 s/min). Exposure to large doses of white light contributes to perovskite film damage as well (*cf.* S117 and S115 with S113). The appropriate GI-WAXS sampling rate must be as high as possible to guarantee good temporal statistics within the same sample and as low as possible to minimize beam damage. Moreover, the GI-WAXS integration time should be as high as possible to guarantee a good signal to noise ratio of the GI-WAXS images and as low as possible to minimize beam damage. For example, a 'realistic' trend of the perovskite peak vs annealing time would be similar to the one of S132, however in this case GI-WAXS patterns are acquired every 10min and with an integration time of 1s. The trends of the $J_{sc}$ (Figure S19c) and $V_{oc}$ (Figure S19c) and the perovskite peaks vs annealing time are similar. However, here beam damage has a lower impact as the interdigitated electrodes extend outside the region probed by the X-ray beam. Therefore, light damage has a stronger influence on the FOM (cf. S115 with S113).

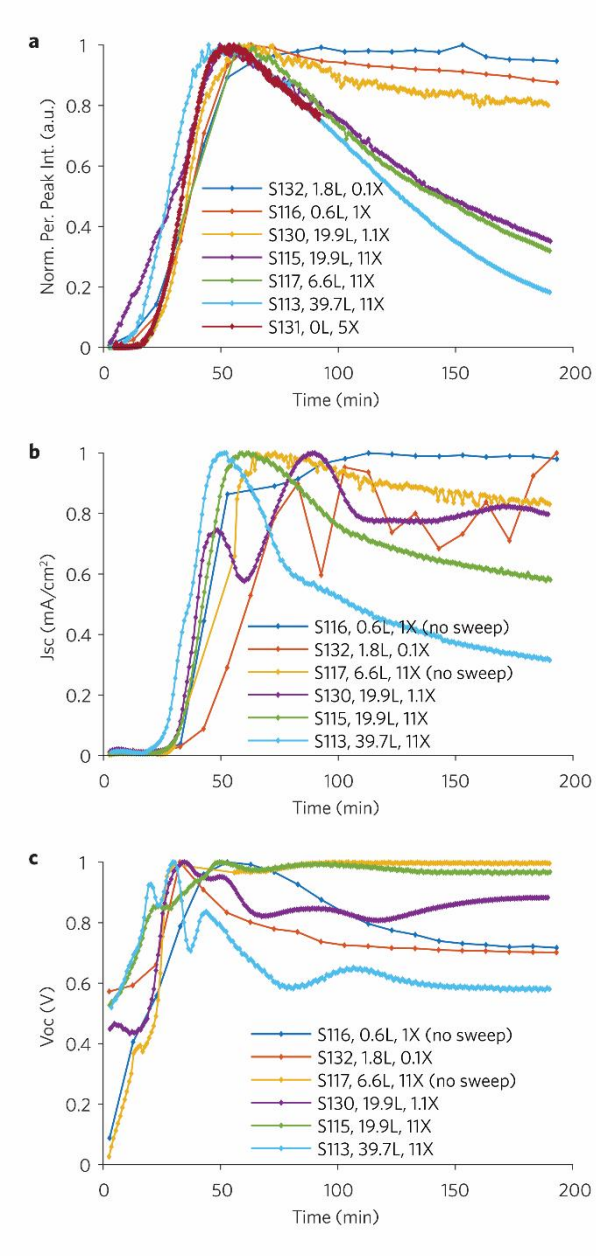


Figure S19 | Effect of X-ray and light damage on (MAI:PbCl2 + HI) IBC solar cells. a, Normalized perovskite peak integrated intensity vs annealing time (see Table S1). b, as a for the normalized short circuit current density. c, as a for the open circuit voltage. In the legends, the light exposure in seconds per minute is followed by 'L', and the X-ray exposure in seconds per minute is followed by 'X'.

## Comparison between IBC and planar solar cells

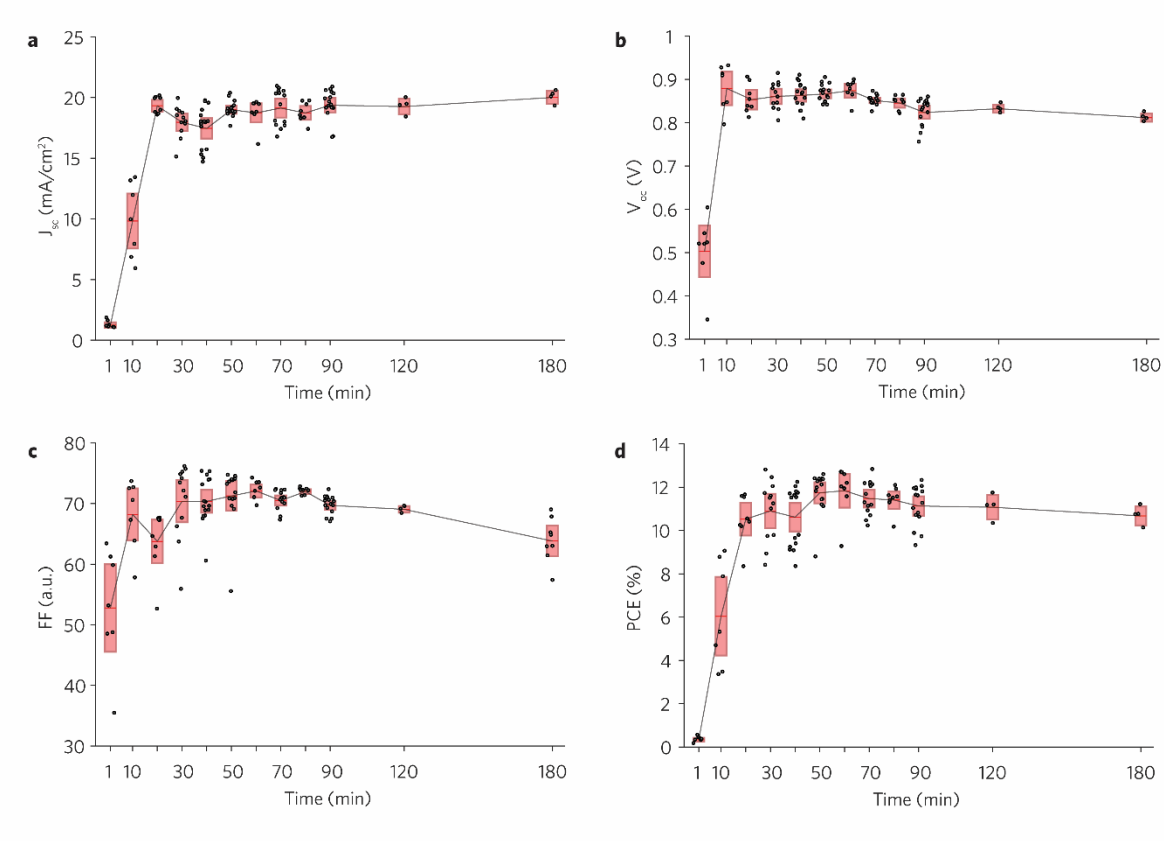


Figure S20 | Figures-of-merit of planar solar cells annealed *ex-situ* at ~97°C. The red bars indicate the average±std for the data points (black dots).

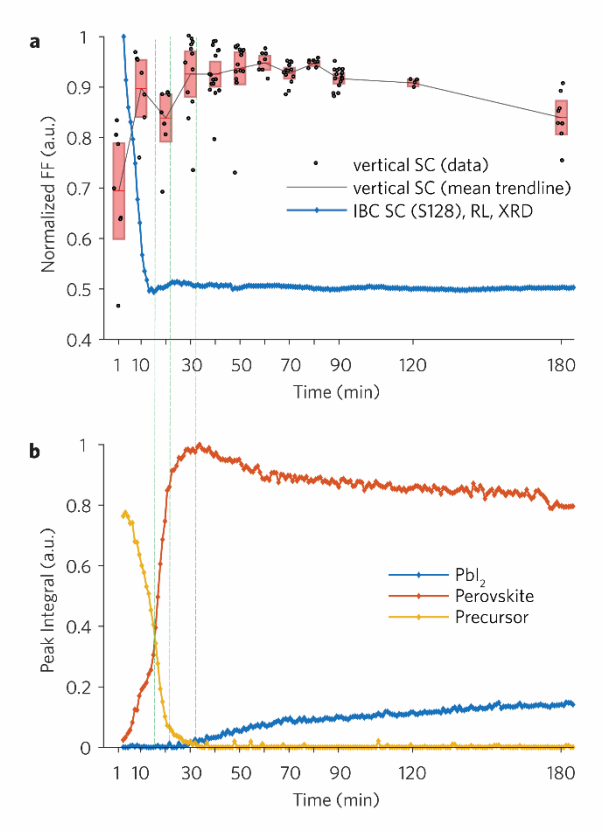


Figure S21 | Normalized fill factor of (MAI:PbCl2 + HI) IBC solar cells annealed *in-situ* and planar solar cell (S128) annealed *ex-situ* at ~97°C and structural data. a, Comparison between normalized FF of IBC S128 and a series of planar solar cells. The red bars indicate the average±std for the data points (black dots). The following measurement procedure for S128 was repeated every 54.4s: measure one GI-WAXS pattern (1s integration time), forward JV sweep (18s, light off), reverse *JV* sweep (18s, light on, indicated as RL). b, Normalized GI-WAXS integrated intensity of the $PbI_2$, perovskite peak, and precursor peak extracted from the azimuthally integrated line profiles. The GI-WAXS data was acquired *in-operando* during the annealing of the IBC solar cell S128.

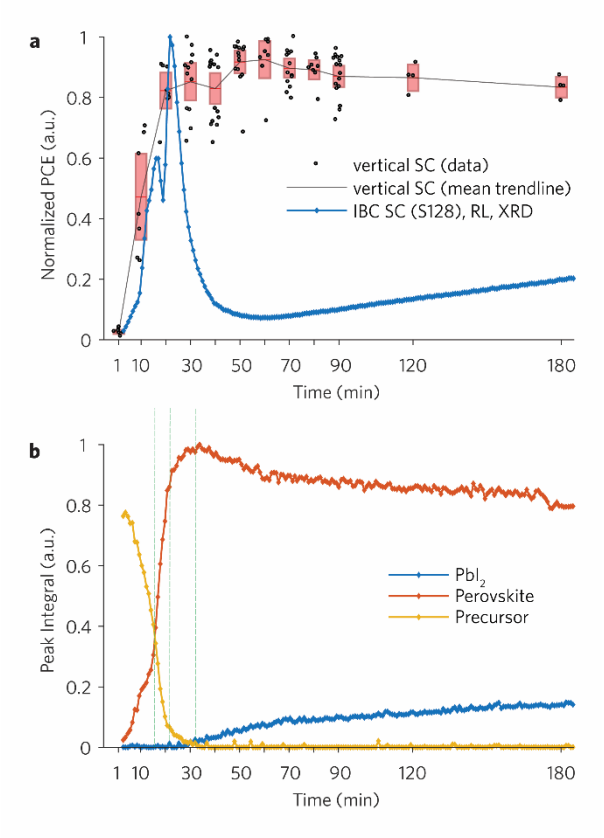


Figure S22 | Normalized power conversion efficiency of (MAI:PbCl2 + HI) IBC solar cell (S128) annealed *in-situ* and planar solar cells annealed *ex-situ* at ~97°C and structural data. a, Comparison between normalized PCE of IBC S128 and a series of planar solar cells. The red bars indicate the average±std for the data points (black dots). The following measurement procedure for S128 was repeated every 54.4s: measure one GI-WAXS pattern (1s integration time), forward JV sweep (18s, light off), reverse *JV* sweep (18s, light on, indicated as RL). b, Normalized GI-WAXS integrated intensity of the $PbI_2$, perovskite peak, and precursor peak extracted from the azimuthally integrated line profiles. The GI-WAXS data was acquired *in-operando* during the annealing of the IBC solar cell S128.

## IBC solar cells fabricated from MAI:$PbCl_2$ with $PbI_2$ additive

We further applied this methodology to a precursor solution based on MAI:$PbCl_2$ (3:0.98) with $PbI_2$ additive (0.5%) dissolved in DMF.[8] Figure S23 illustrates a summary of the *JV* and GI-WAXS measurements performed *in-situ* during the anneal of IBC solar cells at three annealing temperatures (83.8°C, 92.5°C, 114.7°C). The full dataset including diffraction patterns, *JV* measurements, and absolute values of the FOM is available in (Movie S1, S139 - https://youtu.be/ZSUug00lsyU#t=10m54s -, S137 - https://youtu.be/ZSUug00lsyU#t=11m29s -, S158 - https://youtu.be/ZSUug00lsyU#t=11m59s -). Peak integrals of the precursor, perovskite, and lead iodide along with the corresponding normalized FOM for each device are available in Figure S24-Figure S26. Figure S23a shows the integrated peaks of the main perovskite peak, and Figure S23b shows the normalized PCE. Similarly to what was discussed for the HI IBC solar cells, the PCE profile shifts in time with different annealing temperatures. The $J_{sc}$ (Figure S27) starts from very low values, increases, reaches a maximum, and then decreases probably because of the continuous exposure to light. The $V_{oc}$ (Figure S28) initially increases only in the IBC annealed at 114.7°C, whereas for the other two samples, at the beginning, it seems to be quite constant. Then, similarly to the HI IBC devices, the $V_{oc}$ reaches a local minimum, roughly in correspondence of the moment in which the perovskite and precursor peak intensities are comparable (Figure S24-Figure S26). The FF (Figure S29), except for the sample annealed at 83.8°C, reduces in the first instants of the anneal and then stays at relatively stable values. Importantly we notice that the perovskite resulting from this precursor solution, seems to be more resilient to beam damage. For example, the $PbI_2$ signal of IBC S137 ($PbI_2$ additive) annealed at 92.5°C is significantly lower than the $PbI_2$ recorded for IBC S129 (HI additive) annealed under the same conditions (Figure S30).

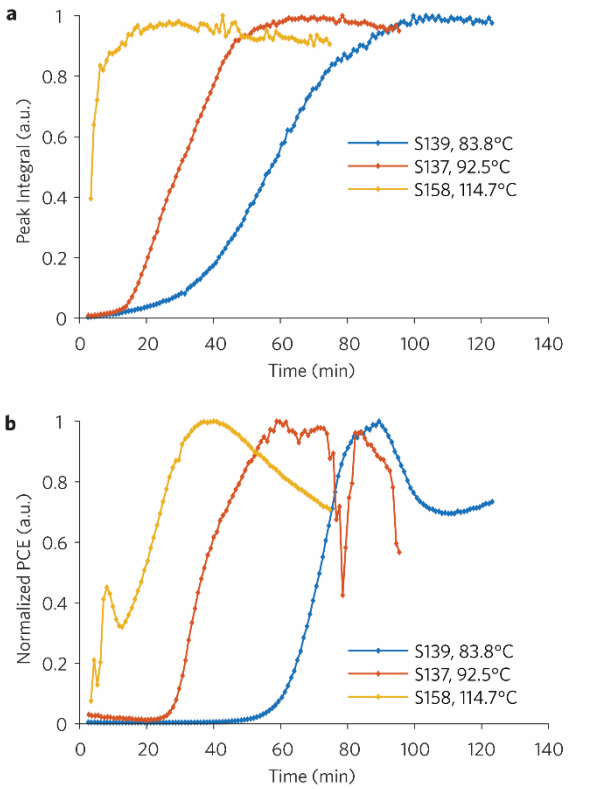


Figure S23 | Perovskite peak integral and normalized PCE extracted from simultaneous GI-WAXS diffraction patterns (dark) and current-voltage (light) measurement of (MAI:$PbCl_2$ + $PbI_2$) IBC solar cells during *in-situ* anneal at 83.8°C, 92.5°C, and 114.7°C. a, Integrated perovskite peak intensities vs annealing time b, Normalized PCE vs annealing time.

The JMA analysis (Figure S31) performed on the perovskite peaks from IBC solar cells annealed at (83.8°C, 92.5°C, 101.6°C, and 114.7°C) reveals that employing $PbI_2$ as an additive in MAI: $PbCl_2$ slows down the precursor to perovskite conversion dynamics, which is indicated by a larger activation energy (94 kJ/mol vs 89 kJ/mol). The inclusion of additives might slow down the conversion speed, although because we annealed the IBC solar cells under nitrogen, this cannot be ruled out. Finally, we also observe grain rotation and lattice expansion or contraction in IBC solar cells fabricated using $PbI_2$ as the additive (Movie S1).

## IBC S139 annealed at 83.8°C

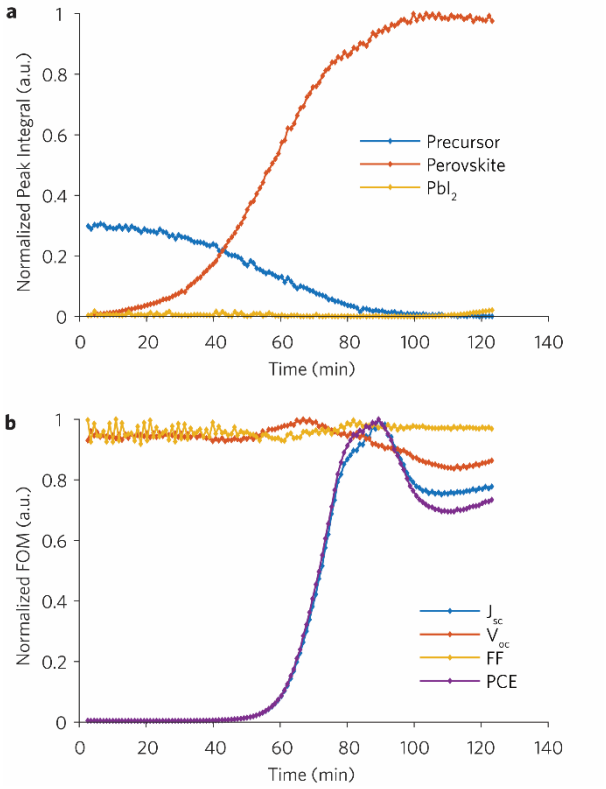


Figure S24 | Structural and opto-electrical parameters extracted from simultaneous GI-WAXS diffraction patterns (dark) and current-voltage (light) measurement of a ($MAI:PbCl_2 + PbI_2$) IBC solar cell (S139) during *in-situ* anneal at 83.8°C. a, Integrated precursor, perovskite and $PbI_2$ peak intensities vs annealing time b, Normalized figures-of-merit (FOM) vs annealing time. The following measurement loop step was repeated every 54.4s: measure one GI-WAXS pattern (1s integration time), forward JV sweep (18s, light off), reverse JV sweep (18s, light on).

## IBC S137 annealed at 92.5°C

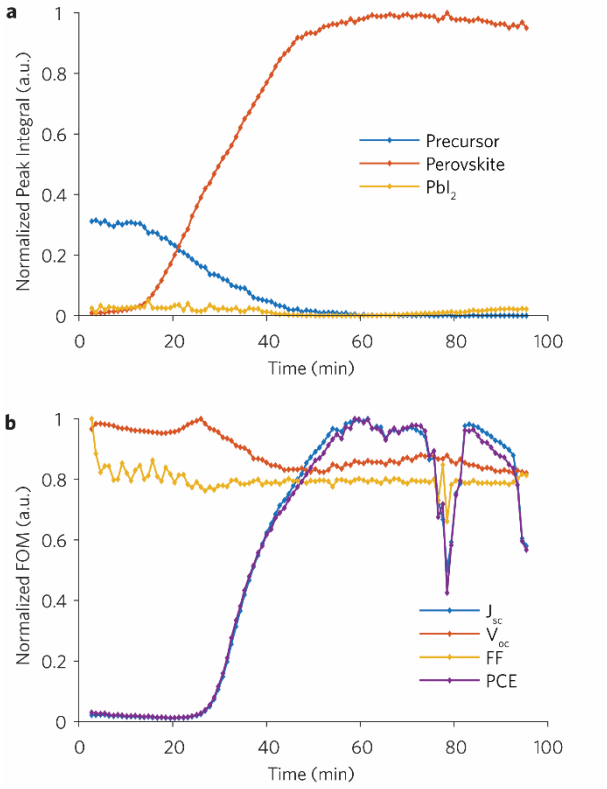


Figure S25 | Structural and opto-electrical parameters extracted from simultaneous GI-WAXS diffraction patterns (dark) and current-voltage (light) measurement of a (MAI:$PbCl_2$ + $PbI_2$) IBC solar cell (S137) during *in-situ* anneal at 92.5°C. a, Integrated precursor, perovskite and $PbI_2$ peak intensities vs annealing time b, Normalized figures-of-merit (FOM) vs annealing time. The following measurement loop step was repeated every 54.4s: measure one GI-WAXS pattern (1s integration time), forward JV sweep (18s, light off), reverse JV sweep (18s, light on).

## IBC 158 annealed at 114.7°C

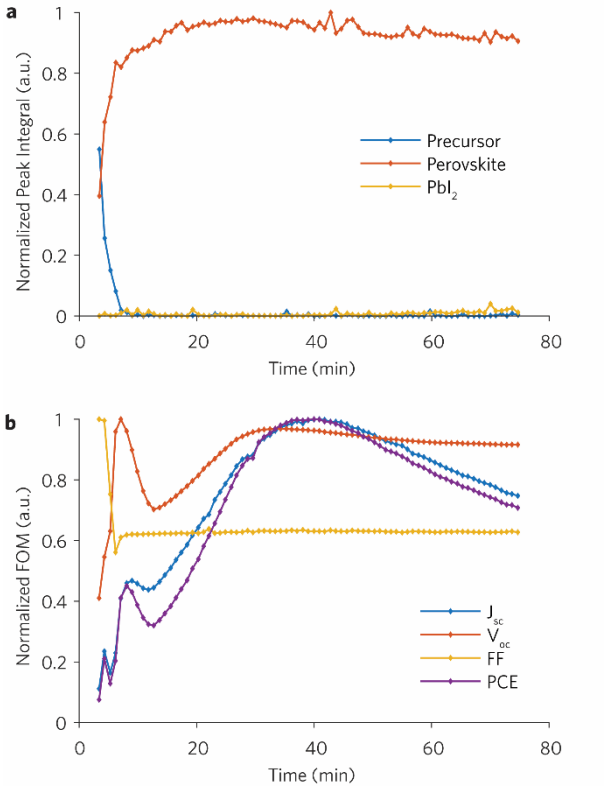


Figure S26 | Structural and opto-electrical parameters extracted from simultaneous GI-WAXS diffraction patterns (dark) and current-voltage (light) measurement of a (MAI:$PbCl_2$ + $PbI_2$) IBC solar cell (S158) during *in-situ* anneal at 114.7°C. a, Integrated precursor, perovskite and $PbI_2$ peak intensities vs annealing time b, Normalized figures-of-merit (FOM) vs annealing time. The following measurement loop step was repeated every 54.4s: measure one GI-WAXS pattern (1s integration time), forward JV sweep (18s, light off), reverse JV sweep (18s, light on).

## Comparison between IBC S139 (83.8°C), IBC S137 (92.5°C), and IBC S158 (114.7°C)

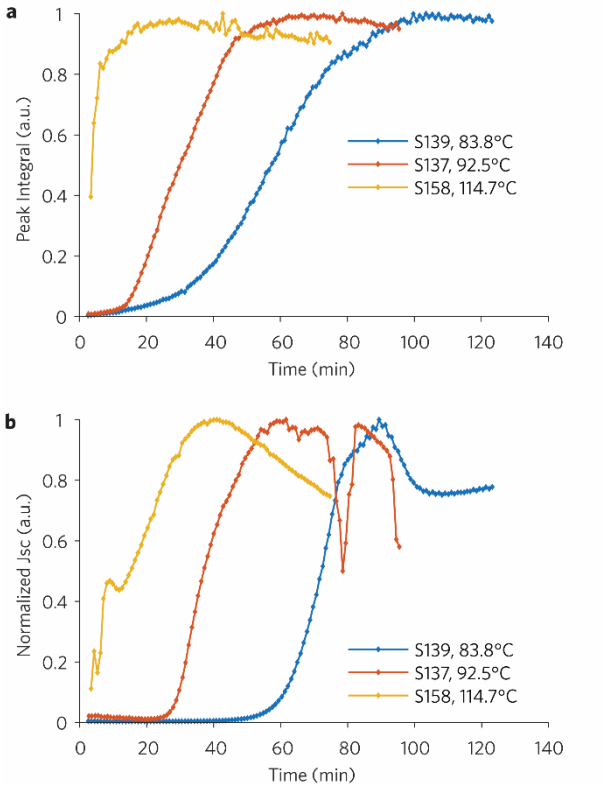


Figure S27 | Perovskite peak integral and normalized $J_{sc}$ extracted from simultaneous GI-WAXS diffraction patterns (dark) and current-voltage (light) measurement of ($MAI:PbCl_2 + PbI_2$) IBC solar cells during *in-situ* anneal at 83.8°C, 92.5°C, and 114.7°C. a, Integrated perovskite peak intensities vs annealing time b, Normalized $J_{sc}$ vs annealing time.

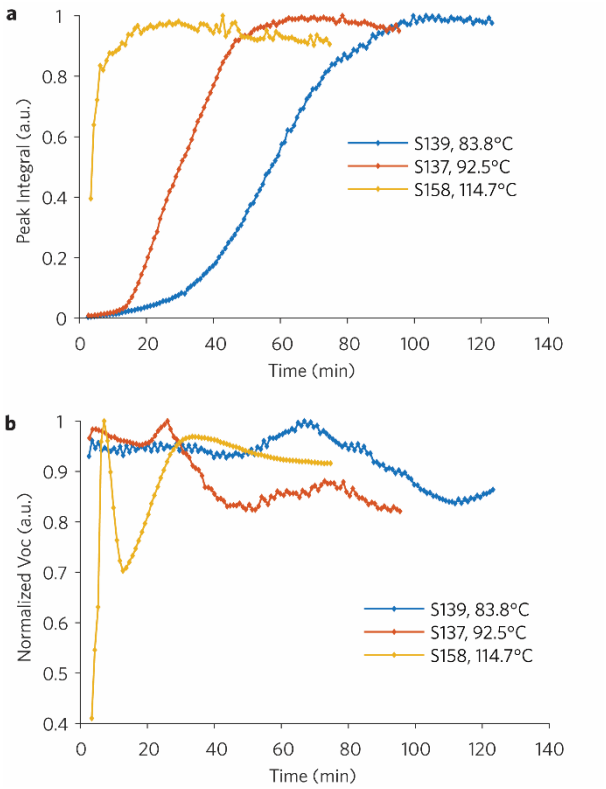


Figure S28 | Perovskite peak integral and normalized $V_{oc}$ extracted from simultaneous GI-WAXS diffraction patterns (dark) and current-voltage (light) measurement of ($MAI:PbCl_2 + PbI_2$) IBC solar cell during *in-situ* anneal at 83.8°C, 92.5°C, and 114.7°C. a, Integrated perovskite peak intensities vs annealing time b, Normalized $V_{oc}$ vs annealing time.

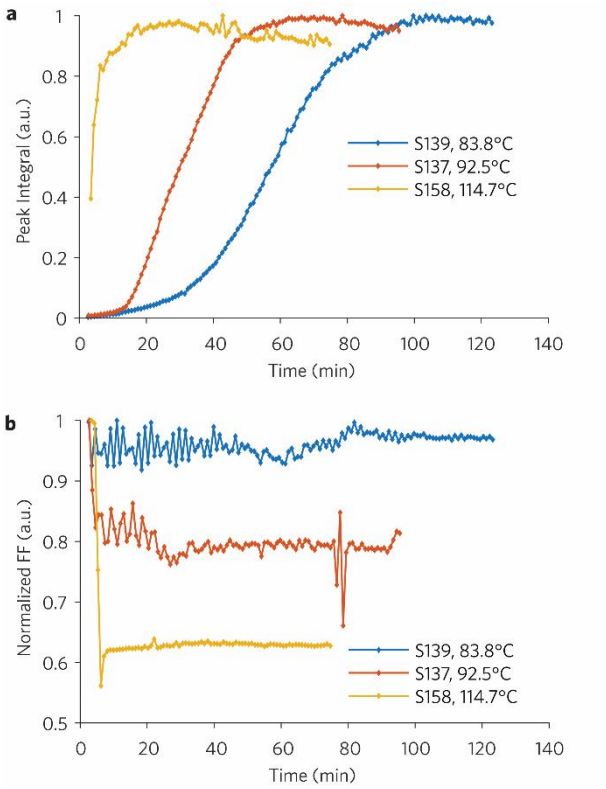


Figure S29 | Perovskite peak integral and normalized FF extracted from simultaneous GI-WAXS diffraction patterns (dark) and current-voltage (light) measurement of ($MAI:PbCl_2 + PbI_2$) IBC solar cell during *in-situ* anneal at 83.8°C, 92.5°C, and 114.7°C. a, Integrated perovskite peak intensities vs annealing time b, Normalized FF vs annealing time.

## $PbI_2$ peak (HI and $PbI_2$ additive)

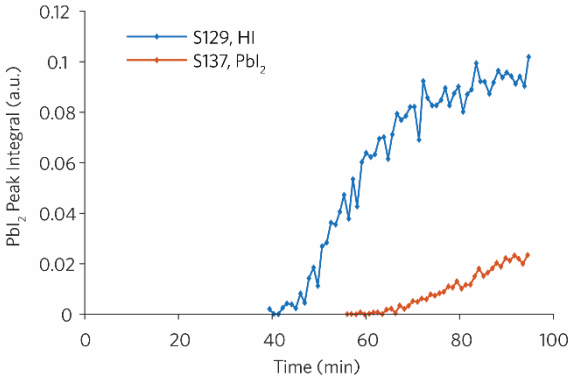


Figure S30 | Comparison between the $PbI_2$ peak integrals of IBC solar cells from MAI:$PbCl_2$ with HI (S129) and $PbI_2$ (S137) additives. The two IBC solar cells were annealed at the same temperature (92.5°C) and measured under the same conditions.

## JMA analysis ($PbI_2$ additive)

Figure S31b shows plots of $\ln(t_{x2}- t_{x1})$, where $t_{x2}$ corresponds to the instants when $x(t)$ is 0.8 and $t_{x1}$ corresponds to the instants when $x(t)$ is 0. From the slope of the line in eq. (1) fittings these data points we obtain an activation energy corresponding to 94±23 kJ/mol.

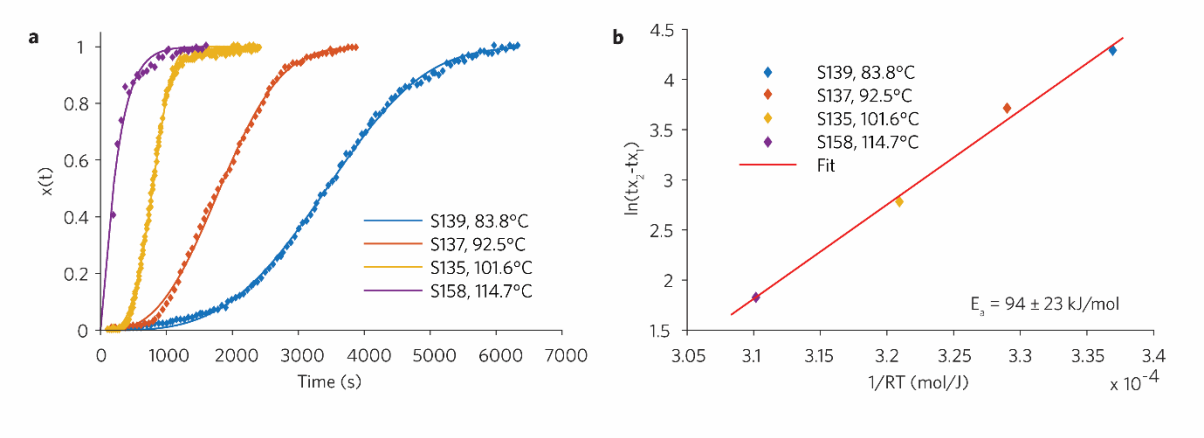


Figure S31 | Kinetic data for isothermally annealed (MAI:$PbCl_2$ + $PbI_2$) IBC perovskite solar cells. a, plots of the perovskite peak integral extracted from azimuthally integrated line profiles for isothermally annealed perovskite solar cells at 83.8°C (blue diamonds), 92.5°C (red diamonds), 101.6°C (yellow diamonds), 114.7°C (violet diamonds), with the JMA model fits (sigmoid in eq. 1, solid lines). b, plots constructed as described in the text and fitted with the line in eq. 1, to extract the slope corresponding to the activation energy $E_a$.

Table S4 | Parameters extracted from the sigmoidal fit of $x(t)$ datapoints in Figure S31a using an activation energy of 94±23 J/mol. $R^2$ is the goodness of the fit.

| **Anneal Temperature (°C)** | ***n*** **(a.u.)** | $k_0$ **(a.u.)** | $R^2$ **(a.u.)** |
|---|---|---|---|
| **83.8** | 3.37±0.05 | $(1.43\pm0.01)\times10^{10}$ | 0.999 |
| **101.6** | 2.86±0.06 | $(1.25\pm0.01)\times10^{10}$ | 0.999 |
| **92.5** | 3.79±0.09 | $(1.40\pm0.01)\times10^{10}$ | 0.998 |
| **114.7** | 1.13±0.20 | $(1.65\pm0.15)\times10^{10}$ | 0.973 |

## IBC solar cell active area

The active area employed for the calculation of the current density and the power conversion efficiency corresponds to the area of the digits facing each other (Figure S32 in red colour) as in ref. [1]. This is the area where the electric field between the PEDOT and $TiO_2$ coated digits is the highest. However, the actual active area could be slightly higher than the 0.0396 $cm^2$ reported here due to extra charges generated outside this region. A more precise calculation of the active area would have involved placing a shadow mask on top of the IBC solar cell, but such a solution was not compatible with the GI-WAXS measurements.

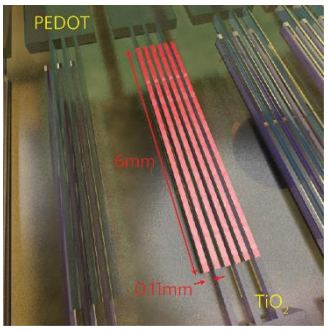


Figure S32 | IBC solar cell active area calculation. The illustration shows the interdigitated area of an IBC solar cell. The digits face each other for 6mm. Each digit is 0.11mm wide. The active area used for the calculations of the current density and the power conversion efficiency is highlighted in red.

## Record Open Circuit Voltage

Table S5 | Record open crcuit voltages for the IBC solar cells measured in this work. Note that in case of forward and reverse sweeps we report the maxium value. Note that S113 is measured during the anneal at 88.2°C and after the anneal at room temperature (24.9°C).

| Sample name | MaxVoc [V] | Measurement Temperature [°C] |
|---|---|---|
| S130 | 0.67 | 88.2 |
| S28 | 0.65 | 88.2 |
| S29 | 0.10 | 88.2 |
| S142 | 0.44 | 83.8 |
| S129 | 0.46 | 92.5 |
| S128 | 0.48 | 96.8 |
| S132 | 0.58 | 88.2 |
| S116 | 0.60 | 88.2 |
| S117 | 0.66 | 88.2 |
| S115 | 0.60 | 88.2 |
| S113 | 0.59 | 88.2 |
| S113d | 0.91 | 24.9 |
| S131 | 0.67 | 88.2 |
| S105 | 0.75 | 96.8 |
| S139 | 0.50 | 83.8 |
| S137 | 0.46 | 92.5 |
| S158 | 0.50 | 114.7 |
| S135 | 0.59 | 101.6 |

## Cake slice

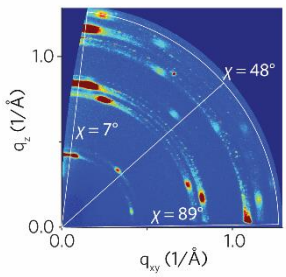


Figure S33 | Cake slice used for the extraction of the azimuthally integrated line profiles. $\chi$ indicates the azimuthal angle.

## References


1 Pazos-Outón, L. M. *et al.* Photon recycling in lead iodide perovskite solar cells. *Science* **351**, 1430-1433 (2016).

2 Tidhar, Y. *et al.* Crystallization of Methyl Ammonium Lead Halide Perovskites: Implications for Photovoltaic Applications. *J. Am. Chem. Soc.* **136**, 13249-13256 (2014).

3 Moore, D. T. *et al.* Crystallization Kinetics of Organic–Inorganic Trihalide Perovskites and the Role of the Lead Anion in Crystal Growth. *J. Am. Chem. Soc.* **137**, 2350-2358 (2015).

4 Barrows, A. T. *et al.* Monitoring the Formation of a CH3NH3PbI3–xClx Perovskite during Thermal Annealing Using X-Ray Scattering. *Adv. Funct. Mater.* **26**, 4934-4942 (2016).

5 Pool, V. L. *et al.* Thermal engineering of FAPbI3 perovskite material via radiative thermal annealing and in situ XRD. *Nat. Commun.* **8**, 14075 (2017).

6 Schelhas, L. T. *et al.* Monitoring a Silent Phase Transition in CH3NH3PbI3 Solar Cells via Operando X-ray Diffraction. *ACS Energy Lett.* **1**, 1007-1012 (2016).

7 Lilliu, S. *et al.* Grain rotation and lattice deformation during perovskite spray coating and annealing probed in situ by GI-WAXS. *CrystEngComm* **18**, 5448-5455 (2016).

8 Sakai, N. *et al.* Controlling Nucleation and Growth of Metal Halide Perovskite Thin Films for High-Efficiency Perovskite Solar Cells. *Small* **13**, 1-8 (2017).